Applied Physics Letters ARTICLE pubs.aip.org/aip/apl

Structural coloration for photovoltaics via sub-monolayer disordered Mie resonators

Cite as: Appl. Phys. Lett. **128**, 224102 (2026); doi: 10.1063/5.0330886
Submitted: 23 February 2026 · Accepted: 18 May 2026 ·
Published Online: 4 June 2026

Zheheng Song,[1,a] Oanh Vu,[2] Jingjian Zhou,[1] Hiroshi Sugimoto,[2] Minoru Fujii,[2] Lars Berglund,[3] and Ilya Sychugov[1,a]

AFFILIATIONS

[1]Department of Applied Physics, KTH Royal Institute of Technology, Stockholm 11419, Sweden
[2]Department of Electrical and Electronic Engineering, Kobe University, Kobe, Hyogo 657-8501, Japan
[3]Department of Fibre and Polymer Technology, KTH Royal Institute of Technology, Stockholm 10044, Sweden

[a)]**Authors to whom correspondence should be addressed:** zheheng@kth.se and ilyas@kth.se

ABSTRACT

Building-integrated photovoltaics (BIPV) are currently hindered by the esthetic trade-off between power conversion efficiency and visual appeal. Conventional colorization methods generally fall into two categories: organic absorption-based dyes, which suffer from high parasitic losses and limited durability, and interference-driven multilayer thin films stacks, which exhibit undesirable iridescence. In this work, we demonstrate highly stable, largely angle-independent color PV modules utilizing a disordered sub-monolayer of dielectric silicon nanoparticles (Si NPs). By leveraging localized Mie resonances within high-index Si nanospheres (100–200 nm in diameter), the angle-dependence of the reflected color is strongly reduced. These Si NPs are encapsulated in a protective polymer shell to prevent clustering, thereby maintaining sharp scattering peaks and color saturation. The nanostructures were deposited via slot-die coating, providing a scalable fabrication route for large-area modules (~50 cm^2 PV devices demonstrated here). Numerical simulations support the experimentally observed spectrally selective reflectance driven by such Si NPs photonic glasses. We achieve a relatively broad CIE 1976 color gamut, including saturated blue, green, and yellowish hues, by varying the size and surface density of Si NPs while maintaining less than 10%–20% relative photocurrent PV loss. This offers a versatile design palette for high-efficiency, esthetically pleasing urban BIPV energy harvesting.

Building-integrated photovoltaics (BIPV) serve as a fundamental technology for energy-harvesting urban surfaces.[1] However, the visual monotony of traditional black or dark-blue solar modules remains a significant barrier to widespread architectural integration.[2,3] To satisfy modern urban design requirements, photovoltaics are expected to evolve from purely functional components into versatile, colorful architectural elements that blend seamlessly into facades and rooftops.[4–7]

The primary challenge in developing colorful PV lies in the fundamental trade-off between esthetic aspects and power conversion efficiency (PCE). Traditionally, color is achieved using pigments or organic dyes.[2,8] They function by absorbing part of the solar spectrum, blocking its conversion into electricity. This parasitic absorption consumes photons that could otherwise generate electricity, significantly reducing PCE and compromising the techno-economic viability of BIPV systems. Furthermore, organic pigments suffer from ultraviolet (UV)-induced degradation, which compromises both the visual appearance and the operational longevity of the module.

An alternative approach involves luminescent downconversion, where materials such as CdSe/ZnS core–shell quantum dots are utilized to convert high-energy ultraviolet (UV) light into longer visible wavelengths.[9] While this method can provide coloration with minimal efficiency loss for specific colors, its benefits are highly device architecture dependent. These luminescent layers are primarily effective for specific solar cell architectures, such as certain heterojunction (HJT) configurations, that may exhibit parasitic absorption or suboptimal internal quantum efficiency in the UV–blue spectral region. In contrast, modern high-efficiency photovoltaic architectures, such as Passivated Emitter and Rear Cell (PERC) or perovskite/silicon tandems, already demonstrate high sensitivity in the short-wavelength regime.[10–12] For these devices, the spectral conversion provides little to no net gain. Crucially, the practical reliability of such luminescent layers is undermined by their response to intense solar radiation; the color saturation often diminishes due to severe quantum yield quenching and thermal instability. Such performance degradation

under standard operating conditions limits their viability for long-term outdoor BIPV applications compared to passive resonant structures.

To achieve efficient spectral control, research has focused on various photonic management strategies. Periodic photonic crystals were explored for their ability to manipulate the density of optical states and generate vivid structural colors through coherent Bragg scattering.[13,14] However, the performance of these periodic structures is intrinsically tied to the periodicity of the lattice, meaning that even minor structural defects or changes in the incident light angle can distort the available modes. As a result, undesired hues and iridescence issues remain.

To overcome these geometric constraints, disordered photonic systems emerge as a compelling alternative for spectrally selective management.[15] Unlike their deterministic periodic counterparts, such photonic glasses rely on the short-range order of scatterers rather than long-range periodicity. This disordered system suppresses the sharp peaks associated with iridescence, offering a path toward angle-independent coloration. Previous studies have utilized multiple scattering in ZnS nanoparticle assemblies to achieve such angle stability.[16] However, heavy reliance on multiple scattering often leads to "whitening" or color desaturation, particularly after module encapsulation. In these systems, light is randomized across a broad spectrum, which diminishes the visual purity and chromatic impact of the PV module.

Crystalline silicon nanoparticles (Si NPs) possess a high refractive index ($n \sim 3.5$–3.7), providing substantial optical contrast against air as well as standard PV encapsulation materials such as ethylene-vinyl acetate (EVA) or glass ($n \sim 1.5$).[17,18] This high index contrast enables exceptionally strong Mie resonant scattering, leading to more vivid and saturated colors compared to previously explored low-index alternatives.[19–21] Furthermore, the covalent bonding of silicon ensures superior chemical and thermal stability compared to organic dyes, satisfying long-term outdoor durability requirements.

In this work, we demonstrate a robust methodology utilizing sub-monolayer disordered silicon nanoparticle photonic glasses (SiPG) as high-index resonant structures. By modulating the Si NPs' size from 100 to 200 nm, we achieve highly saturated colors across the visible spectrum. Specifically distinct blue, green, and yellow hues were produced on standard Si PV modules. Finite Element Method (FEM) simulations reveal how the scattering cross sections scale with NP size to define the spectral response. To maintain peak saturation, we utilize a sub-monolayer distribution that suppresses parasitic multiple scattering typically caused by nanoparticle clustering. To prevent agglomeration during the coating process and preserve the narrow resonant linewidth, the Si NPs are encapsulated in poly(N-isopropylacrylamide) (PNIPAM) shells. These shells provide steric hindrance to ensure particle separation, which suppresses interparticle coupling and preserves optically independent Mie resonances, resulting in narrower spectral features. It was shown previously that at an interparticle separation of ~100 nm or greater, the NPs act optically close to individual scatterers. In the absence of aggregation-prevention measures, large clusters of NPs can form, with a complete loss of the selective scattering function.[22] This precise control over the nanostructure surface density maximizes color purity while minimizing optical interference (fabrication details are provided in the Methods section of the supplementary material). The SiPG is integrated onto the inner surface of the module cover glass, relying on the glass itself as a hermetic protection layer. This configuration ensures environmental stability and enables seamless integration with standard PV architectures without modifying the cell-level fabrication process. By decoupling the colorization layer from the active semiconductor, this strategy provides a robust and scalable solution for urban energy harvesting, offering minimal energy cost for coloration (~10%–20% of the photocurrent).

The architectural layout of the SiPG-enhanced color PV module is schematically depicted in Fig. 1(a). The system features a sub-monolayer of Si NPs deposited onto the interior surface of the protective cover glass, which is then coupled to the silicon solar cell via an EVA encapsulant layer. This "bottom-side" deposition strategy is vital for BIPV durability; the cover glass serves as an intrinsic physical shield, isolating the resonant nanostructures from mechanical abrasion and environmental contamination.

The underlying optical mechanism was investigated using the Finite Element Method (FEM). Figure 1(b) displays the calculated backscattering (BS), forward scattering (FS), and absorption (ABS) cross sections for a representative 140 nm diameter Si NP on glass. The spectrum reveals a dominant BS peak in the green spectral region, confirming the efficacy of Si NPs as low-loss dielectric resonators. Notably, the absorption cross section remains small relative to the scattering cross section across the visible range—a fundamental

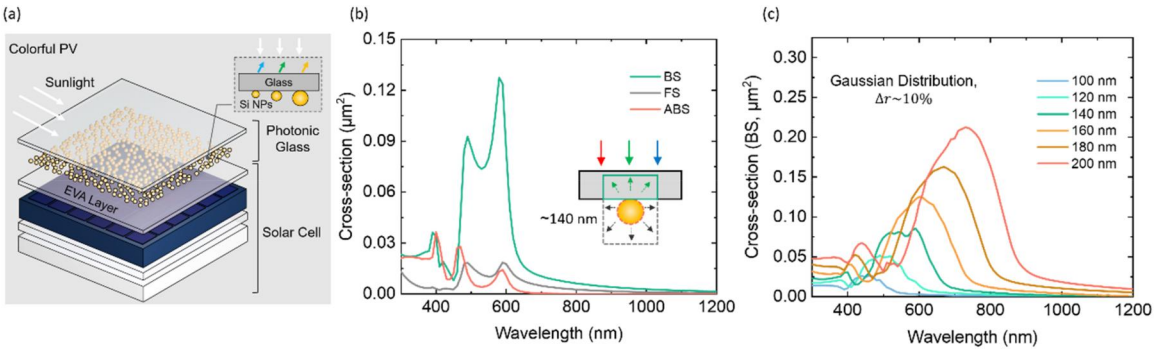

FIG. 1. Structural design and Mie resonances of Si NP-enhanced color PV modules. (a) Schematic of the colorful PV module featuring a sub-monolayer of Si NPs at the glass/EVA interface. (b) Calculated scattering and absorption cross sections for a single 140 nm Si NP. (c) Size-dependent BS spectra for Si NP ensembles with average diameters from 100 to 200 nm.

prerequisite for achieving high-saturation color without compromising much of device PCE.

To evaluate spectral tunability, the size-dependent backscattering response was simulated for Si NPs on glass with diameters ranging from 100 to 200 nm, as shown in Fig. 1(c). As the particle size increases, the primary BS peaks undergo a significant redshift and spectral broadening. Furthermore, the emergence of higher-order resonant modes is observed in the shorter wavelength regime for larger particles like 200 nm Si NPs. This simulation underscores a fundamental constraint in Mie-based structural color: achieving saturated red hues purely through a particle scattering mechanism is challenging. The higher-order BS peaks (quadruple modes) of red-resonant particles inevitably encroach upon the blue spectral region, potentially desaturating the perceived color. This theoretical insight guides the selection of the 100–200 nm diameter range for achieving saturated primary hues.

The morphological and visual characteristics of the resonant nanostructures are presented in Fig. 2. Figure 2(a) shows the high-resolution transmission electron microscopy (TEM) and atomic force microscopy (AFM) images of the pure Si NPs and the structures after slot-die coating with a diameter of 140 nm. Thanks to the post-synthesis size separation method, the AFM image demonstrates spatial isolation, which is critical for maintaining the purity of the individual Mie resonance modes and preventing the spectral broadening associated with near-field coupling. Indeed, our previous work demonstrates that when the inter-particle distance exceeds ~100 nm,[22] the scattering cross section of a two-particle system almost equals the sum of two independent Si NPs, justifying the treatment of these nanostructures as individual scattering centers.

The photographs in Fig. 2(b) reveal the distinct color profiles of the SiPGs after slot-die deposition onto glass substrates with a surface density of ~7.5 NPs μm^{-2}. The perceived color is dominated by the back-scattered/reflected light. We observe representative size-dependent coloration: samples with diameters of 110, 120, 140, 170, and 200 nm exhibit vivid blue, cyan, green, and yellowish-orange hues, respectively. Beyond a diameter of 170 nm, the size-dependent color saturation diminishes. Here, instead, an orange or brownish hue appears as the primary resonance redshifts out of the visible peak sensitivity region and higher-order modes begin to dominate. All photographs were captured against a non-reflective black velvet background to eliminate stray light interference. A standard white reference was placed within the frame (not shown) to facilitate consistent white balance calibration across all samples in the camera. As also illustrated in the photographs in Fig. 2(b), the samples maintain a consistent color profile even at different oblique viewing angles. When observed at extreme tilted angles, the samples do not exhibit the radical iridescence typical of periodic photonic structures. This enhanced angular stability confirms that the optical response is spatially dominated by individual Mie resonances rather than collective Bragg diffraction. By leveraging the short-range order of the photonic glass, we successfully decouple the spectral reflectance from the incident angle, satisfying a critical requirement for consistent BIPV esthetics in varied urban lighting conditions.

The influence of surface density on the optical response is quantified in Fig. 2(c). We varied the density across four levels ~2.5, ~5.0, ~7.5, and ~10.0 NPs μm^{-2}, with values verified through statistical analysis of AFM images (see Fig. S1). As the surface density increases, we observe a slight spectral shift in the resonant peak, likely due to subtle changes in the effective refractive index of the layer. However, the most prominent effect is the substantial increase in reflection intensity. For our standard device configuration, we selected a density of ~7.5 NPs μm^{-2}. This density optimizes the balance between color saturation and transparency, ensuring a robust sub-monolayer distribution that avoids the formation of overlayers or dense clusters. Using this optimized density, we characterized the spectral tunability for different Si NPs diameters. Figure 2(d) presents the transmittance and reflectance spectra for such films with Si NP diameters of 110, 120, 140, 170, and 200 nm. The systematic redshift of both the transmission minima and reflectance maxima validates the diameter-dependent Mie scattering mechanism. Photographic evidence in Fig. S2 validates the distinct optical transmission and reflection modes of the SiPGs across varying surface densities. This architecture facilitates spectrally selective reflectance for esthetic coloration without compromising high transmittance, thereby ensuring that maximum solar flux reaches the underlying PV cell for efficient energy harvesting. As demonstrated in Fig. S3, the corresponding spectral response is further tunable via the Si NP surface density, enabling precise control over color saturation and transparency. These findings confirm that the SiPG system offers a versatile platform for BIPV coloration, allowing for tailored wavelength targeting through surface density modulation and geometric scaling.

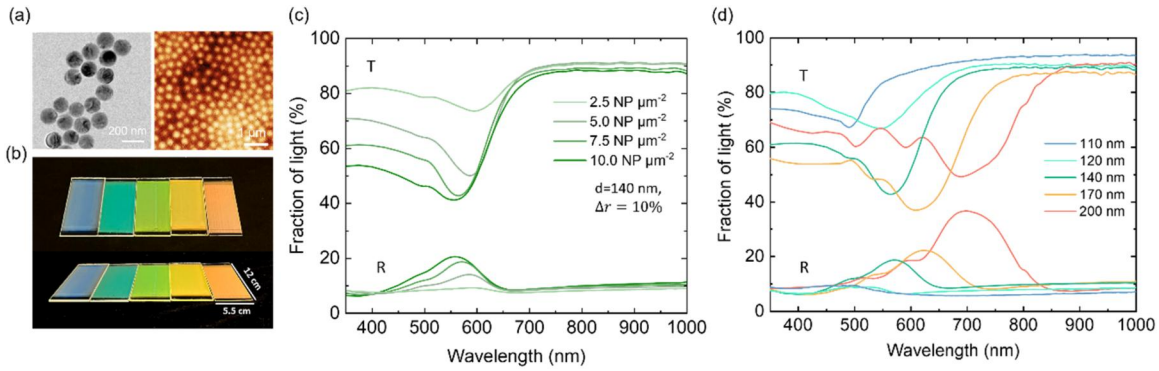

FIG. 2. Morphological characterization and angle-independent Mie coloration. (a) TEM and AFM images of 140 nm Si NPs. (b) Photographs of SiPGs across varying diameters and viewing angles. (c) Density-dependent reflectance spectra (2.5–10.0 NPs μm^{-2}). (d) Diameter-dependent transmittance and reflectance spectra.

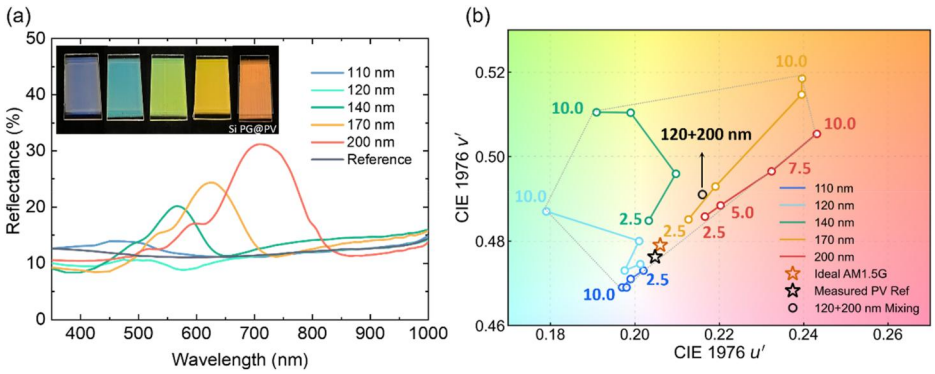

FIG. 3. Visual performance and chromaticity analysis of SiPG@PV modules. (a) Reflectance spectra of integrated SiPG@PV modules with varying Si NP diameters; the inset shows photographs of the completed colorful modules. (b) Chromaticity coordinates mapped on the enlarged CIE 1976 (u′, v′) diagram for different particle sizes and surface densities (2.5–10.0 NPs μm^{-2}). Theoretical color gamut (dotted gray area) achievable via the SiPG method by tuning nanoparticle diameter and surface density.

The visual and spectral characteristics of the integrated SiPG@PV (~7.5 NPs μm^{-2}) modules are further evaluated in Fig. 3. Photographs of the completed devices [Fig. 3(a)] demonstrate vivid, uniform coloration for modules featuring 110, 120, 140, 170, and 200 nm Si NPs when integrated with a standard silicon solar cell module (5.5 × 9.0 cm^2). These spectra represent the reflectance spectra of these integrated devices. Compared to the standalone SiPG, the reflectance intensity is only slightly attenuated due to the high absorption of the underlying solar cell and the coupling and interaction with the solar cell top encapsulant. Crucially, these resonance peaks positions remain spectrally stationary, confirming that the localized Mie mechanism is robust against integration-induced optical environment changes. To further investigate the impact of integration on optical performance, we analyzed the reflectance evolution of the SiPG@PV devices as a function of surface density across all sizes (Fig. S4). As observed in the supplementary material data, increasing the density from ~2.5 to 10.0 NPs μm^{-2} leads to a significant and non-linear enhancement in reflectance intensity for all wavelengths, allowing for flexible esthetic matching for different architectural needs.

The resulting color gamut is mapped in the CIE 1976 (u′, v′) uniform chromaticity scale in Figs. 3(b) and S5. We utilize the CIE 1976 system because its perceptual uniformity allows for a more accurate representation of color differences compared to the CIE 1931 space.[23] The chromaticity coordinates, converted from the measured reflectance spectra, show a relatively broad range of achievable colors. In the center of the chromaticity diagram, we denote the reference points with star symbols: the orange star represents the ideal PV reference, while the black star indicates our measured PV reference. Both references are positioned near the neutral white point (center), serving as the baseline from which our Si NP-integrated modules diverge into specific color series. The enlarged details in Fig. 3(b) track the coordinates for the 110, 120, 140, 170, and 200 nm series. The systematic shift of the coordinates from the central neutral point toward the blue, green, and orange-red regions with increasing surface density validates the coloration functionality of the Si NP-based photonic glasses.

The practical utility of SiPG technology is evaluated through its photo-electrical performance under standard operating conditions. To simulate a realistic working environment, all SiPG@PV modules were pre-conditioned under 1-sun illumination to reach thermal equilibrium before measurement. This steady-state temperature regime ensures the stability of the efficiency metrics, confirming that the photovoltaic response remains consistent once the device reaches its operating temperature. The corresponding current–voltage (I–V) characteristics are presented in Fig. 4(a). Figure 4(b) presents the wavelength-dependent External Quantum Efficiency (EQE) loss. The primary photocurrent losses are confined to the visible spectral range, directly correlating with the resonant backscattering bands of the Si NPs. Detailed EQE curves for different particle sizes and surface densities can be found in Fig. S6.

As Mie-resonant SiPG primarily influences photon trajectories rather than the internal carrier recombination physics, the open-circuit

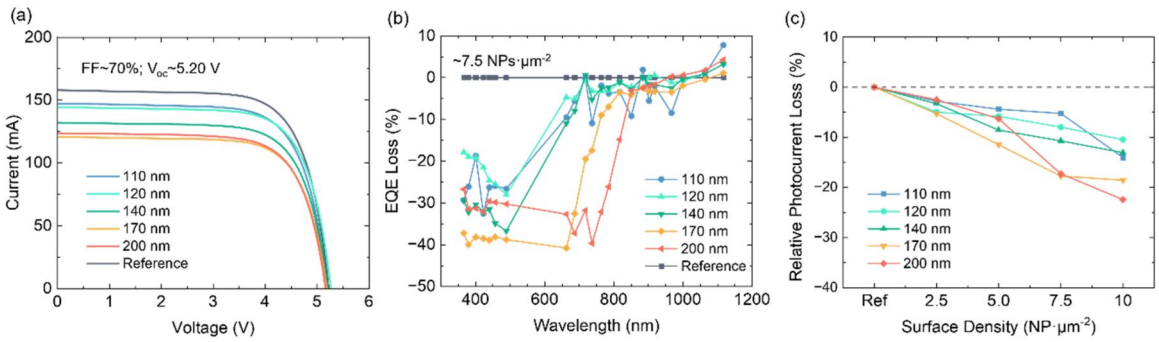

FIG. 4. Photovoltaic performance and optoelectronic losses of SiPG@PV modules. (a) I–V characteristics of SiPG@PV modules. (b) Wavelength-dependent EQE loss at a surface density of 7.5 NPs μm^{-2}. (c) Relative photocurrent loss as a function of Si NP surface density for different particle sizes.

voltage (V_{oc}) remains largely unaffected. We therefore focus on the relative short-circuit current loss. The correlation between relative total photocurrent loss, surface density, and size of Si NPs is quantified in Fig. 4(c). Across all color series, the relative losses are predominantly maintained below 20%. Notably, at the optimized surface density of ~7.5 NPs μm^{-2}, the relative loss is constrained, while providing saturated esthetic output. For example, clear blue, green, and cyan colors can be realized with less than 10% photocurrent loss.

Furthermore, color mixing experiments are detailed in Figs. 3(b) and S7. By blending 120 and 200 nm Si NPs, we demonstrate the generation of intermediate spectral signatures, effectively bridging the gap between blue and orange hues. In principle, through precise stoichiometric mixing, this approach allows for an expanded color palette, theoretically covering the entire chromatic range between the primary scattering peaks. Finally, Fig. S8 presents the relationship between relative photocurrent loss and the CIELAB L^* (lightness) value. Our results demonstrate that the SiPG system achieves acceptable visual lightness, reaching the L^* 40–50 range with minimal electrical penalties. This balance is superior to traditional methods, as it allows for vivid, human-perceivable colors on building facades without the excessive energy loss typically caused by opaque pigments or broad-band interference filters.

In summary, we have demonstrated a scalable and robust methodology for achieving angle-independent structural coloration in photovoltaics using sub-monolayer silicon nanoparticle photonic glasses (SiPG). By leveraging localized Mie resonances in high-index polycrystalline Si NPs (100–200 nm), we decoupled color appearance from the incident sunlight and viewing angles, effectively reducing the iridescence common in conventional interference filters. Crucially, the intrinsic chemical stability of Si NPs combined with slot-die coating enables uniform deposition of sub-monolayers over large areas, facilitating a reliable scale-up. Our integrated SiPG@PV modules achieved saturated primary and secondary hues with a relatively broad color gamut in the CIE 1976 (u′, v′) space while keeping relative efficiency losses below 20% (below 10% for the blue and green range). With a demonstrated lightness (L^*) of 40–50, this SiPG technology provides a practical, industrially compatible solution for high-performance building-integrated photovoltaics.

See the supplementary material for additional experimental and simulation details, nanoparticle synthesis and slot-die coating procedures, AFM characterization, density-dependent optical spectra, chromaticity analysis, EQE measurements, color-mixing experiments, and the correlation between relative loss and lightness.

The authors acknowledge funding from the Knut and Alice Wallenberg Foundation through Grant KAW 2021.0311. Z.S. acknowledges funding support from the China Scholarship Council (CSC). This work is partially supported by the Japan Society for the Promotion of Science (JSPS) Bilateral Joint Research Project (JPJSBP120249928) and the Kobe University Strategic International Collaborative Research Grant. H.S. acknowledges support from JST Grant Nos. JPMJPF2503 and JPMJSF2405. We thank Professor Muhammet Toprak and Dr. Jose Serrano for helping with the slot-die coater.

AUTHOR DECLARATIONS

Conflict of Interest

The authors have no conflicts to disclose.

Author Contributions

Zheheng Song: Conceptualization (equal); Data curation (equal); Formal analysis (equal); Funding acquisition (equal); Investigation (equal); Methodology (equal); Project administration (equal); Resources (equal); Software (equal); Validation (equal); Visualization (equal); Writing – original draft (equal); Writing – review & editing (equal). **Oanh Vu:** Conceptualization (lead); Data curation (equal); Formal analysis (equal); Funding acquisition (lead); Investigation (equal); Methodology (equal); Project administration (equal); Resources (equal); Software (equal); Supervision (equal); Validation (equal); Writing – review & editing (equal). **Jingjian Zhou:** Formal analysis (supporting); Investigation (supporting); Methodology (supporting); Resources (equal); Validation (equal); Writing – review & editing (supporting). **Hiroshi Sugimoto:** Data curation (equal); Funding acquisition (equal); Investigation (equal); Methodology (equal); Resources (equal); Supervision (equal); Validation (equal); Writing – review & editing (equal). **Minoru Fujii:** Data curation (equal); Formal analysis (equal); Funding acquisition (equal); Investigation (equal); Methodology (equal); Project administration (equal); Resources (equal); Supervision (equal); Writing – review & editing (equal). **Lars Berglund:** Data curation (equal); Formal analysis (equal); Funding acquisition (equal); Methodology (equal); Project administration (equal); Supervision (equal); Writing – review & editing (equal). **Ilya Sychugov:** Conceptualization (lead); Data curation (equal); Formal analysis (lead); Funding acquisition (lead); Investigation (equal); Methodology (equal); Project administration (equal); Resources (equal); Software (equal); Supervision (equal); Validation (equal); Writing – review & editing (equal).

DATA AVAILABILITY

The data that support the findings of this study are available from the corresponding authors upon reasonable request.

REFERENCES

[1]N. Martín Chivelet, C. Kapsis, and F. Frontini, *Building-Integrated Photovoltaics: A Technical Guidebook*, 1st ed. (Routledge, New York, 2024).
[2]Z. Li, S. Li, J. Yan, J. Peng, and T. Ma, "Balancing aesthetics and efficiency of coloured opaque photovoltaics," Nat. Rev. Clean Technol. **1**(3), 216–226 (2025).
[3]A. Faes, A. Virtuani, H. Quest, L. Maturi, A. Scognamiglio, F. Frontini, A. Schlueter, N. Martin-Chivelet, A. Reinders, and C. Ballif, "Building-integrated photovoltaics," Nat. Rev. Clean Technol. **1**(5), 333–350 (2025).
[4]J. Huang, J. Zhou, T. Haraldsson, A. Clemments, M. Fujii, H. Sugimoto, B. Xu, and I. Sychugov, "Triplex glass laminates with silicon quantum dots for luminescent solar concentrators," Sol. RRL **4**(9), 2000195 (2020).
[5]J. Huang, J. Zhou, E. Jungstedt, A. Samanta, J. Linnros, L. A. Berglund, and I. Sychugov, "Large-area transparent 'quantum dot glass' for building-integrated photovoltaics," ACS Photonics **9**(7), 2499–2509 (2022).
[6]I. Sychugov, "Analytical description of a luminescent solar concentrator," Optica **6**(8), 1046 (2019).
[7]K. Lee, N. Kim, K. Kim, H.-D. Um, W. Jin, D. Choi, J. Park, K. J. Park, S. Lee, and K. Seo, "Neutral-colored transparent crystalline silicon photovoltaics," Joule **4**(1), 235–246 (2020).

[8]A. Soman, R. Jadhav, and A. Antony, "Review on the progress of colored silicon solar cells for building-integrated photovoltaics (BIPV) application," Sustainable Energy Technol. Assess. **83**, 104612 (2025).
[9]C. Jiang, G. Zhang, Z. Hong, J. Chen, Y. Li, X. Yuan, Y. Lin, C. Yu, T. Wang, T. Song, Y. Wang, and B. Sun, "Colored silicon heterojunction solar cells exceeding 23.5% efficiency enabled by luminescent down-shift quantum dots," Adv. Mater. **35**(6), 2208042 (2023).
[10]E. Aydin, E. Ugur, B. K. Yildirim, T. G. Allen, P. Dally, A. Razzaq, F. Cao, L. Xu, B. Vishal, A. Yazmaciyan, A. A. Said, S. Zhumagali, R. Azmi, M. Babics, A. Fell, C. Xiao, and S. De Wolf, "Enhanced optoelectronic coupling for perovskite/silicon tandem solar cells," Nature **623**(7988), 732–738 (2023).
[11]S. Wang, W. Li, C. Yu, W. Shi, Q. Kang, F. Cao, K. Gao, L. Yang, B. Yang, J. Zhou, S. Yang, Q. Wang, Q. Fei, X. Chen, G. Chen, P. Chen, Z. Li, W.-C. Hsu, Z. Yan, Y. Bai, W. Liu, S. De Wolf, X. Yang, and X. Zhang, "Flexible perovskite/silicon tandem solar cells with 33.6% efficiency," Nature **649**(8095), 59–64 (2026).
[12]C. Xing, W. Gu, K. Gao, B. Shao, C. Jiang, G. Bai, D. Xu, X. Wang, K. Li, Z. Song, Z. Su, J. Mao, X. Zhang, P. Zheng, W. Zhang, X. Zhang, Y. Wang, X. Yang, and B. Sun, "Electron-selective strontium oxide contact for crystalline silicon solar cells with high fill factor," Sol. RRL **7**(9), 2201100 (2023).
[13]C. G. Ferreira, J. Lamminaho, A. Paul, M. Babin, N. L. Andersen, S. Thorsteinsson, P. B. Poulsen, K. Petersons, L. Yde, J. F. Stensborg, N. A. Mortensen, J. D. Cox, and M. Madsen, "Optical design of structural colored photovoltaics for building integration: From periodic configurations to optimization algorithms," Nano Energy **148**, 111659 (2026).
[14]S. Li, Y. Chen, T. Li, Z. Li, and T. Ma, "Multilayer thin film design for neutral-colored opaque photovoltaics," Appl. Energy **378**, 124710 (2025).
[15]Z. Li, T. Ma, Y. Chen, S. Li, Y. Dai, D. Zhang, H. Yang, and J. Yan, "Structural coloring of solar photovoltaics with quasi-ordered photonic pigments," Nexus **2**(4), 100101 (2025).
[16]Z. Li, T. Ma, S. Li, W. Gu, L. Lu, H. Yang, Y. Dai, and R. Wang, "High-efficiency, mass-producible, and colored solar photovoltaics enabled by self-assembled photonic glass," ACS Nano **16**(7), 11473–11482 (2022).
[17]J. Song, H. Tanaka, K. Moriasa, H. Sugimoto, and M. Fujii, "Mie-resonant structural color of silicon nanosphere monolayer coupled with Fabry–Pérot cavity," ACS Appl. Opt. Mater. **2**(7), 1420–1426 (2024).
[18]O. Vu, K. Ozawa, M. K. Habil, H. Sugimoto, and M. Fujii, "Immobilization of Mie-resonant silicon nanospheres on a silica substrate for surface-enhanced fluorescence," Adv. Opt. Mater. **13**, 2402808 (2025).
[19]O. Vu, J. Song, H. Sugimoto, and M. Fujii, "Polymer-shell coating of Mie-resonant silicon nanospheres for controlled fabrication of self-assembled monolayer," ACS Appl. Nano Mater. **8**(29), 14802–14810 (2025).
[20]H. Tanaka, S. Hotta, T. Hinamoto, H. Sugimoto, and M. Fujii, "Monolayer of Mie-resonant silicon nanospheres for structural coloration," ACS Appl. Nano Mater. **7**(3), 2605–2613 (2024).
[21]Y. H. Fu, A. I. Kuznetsov, A. E. Miroshnichenko, Y. F. Yu, and B. Luk'yanchuk, "Directional visible light scattering by silicon nanoparticles," Nat. Commun. **4**(1), 1527 (2013).
[22]Z. Song, X. Lu, O. Vu, J. Song, H. Sugimoto, M. Fujii, L. Berglund, and I. Sychugov, "Selective scatterers improve efficiency and color neutrality of semi-transparent photovoltaics," ACS Photonics **12**(11), 6458–6467 (2025).
[23]C. Yang, D. Liu, M. Bates, M. C. Barr, and R. R. Lunt, "How to accurately report transparent solar cells," Joule **3**(8), 1803–1809 (2019).

Supporting Information

Structural Coloration for Photovoltaics via Submonolayer Disordered Mie Resonators

Zheheng Song[1*], Oanh Vu[3], Jingjian Zhou[1], Hiroshi Sugimoto[3], Minoru Fujii[3], Lars Berglund[2] and Ilya Sychugov[1*]

[1] Department of Applied Physics, KTH Royal Institute of Technology, Stockholm 11419 Sweden

[2] Department of Fibre and Polymer Technology, KTH Royal Institute of Technology, Stockholm 10044, Sweden

[3] Department of Electrical and Electronic Engineering, Kobe University, 657-8501, Japan

*ilyas@kth.se, *zheheng@kth.se

1. Methods

Numerical modeling was performed using COMSOL Multiphysics 6.3 where the finite element method (FEM) was employed to solve the Helmholtz equation for individual Si NPs on glass. The model utilized the wavelength-dependent complex refractive index of crystalline Silicon. To simulate the experimental silicon nanoparticle photonic glasses (SiPG) response, individual scattering profiles for a given size were convoluted with a Gaussian size distribution using experimental standard deviation value of ~ 10% of the average size.[1]

Si NPs were obtained from SiO-derived silicon-rich oxide using a high-temperature phase-separation route. The precursor was annealed at 1500 °C for 30 min in nitrogen, which generated Si-rich crystalline domains embedded in an oxide matrix. The oxide phase was subsequently removed by HF treatment for 1 h, releasing polycrystalline Si NPs that were collected and dispersed in methanol. Particle-size selection was then carried out by density-gradient centrifugation in sucrose. In a typical separation, 1.8 mL of the methanol-based Si NP suspension was loaded into the sucrose medium and centrifuged at 5500 rpm for 55–60 min. The separated fractions were withdrawn from the top in 1 mL portions and stored individually. To remove residual sucrose, the collected fractions were repeatedly rinsed with water before being exchanged into methanol. A PNIPAM microgel shell was polymerized on propyl methacrylate (MPS) functionalized Si NPs via a radical polymerization process. Size-selected Si NP suspensions with a final concentration of approximately 1 mg/mL were washed several times with DI and stored in anhydrous ethanol.[2]

For slot-die coating, the particle coverage on glass was tuned through the Si NP ink concentration and the number of repeated coating passes (N). The deposition was conducted at a fixed substrate temperature of 50°C and a coating speed of 5 mm/s. The core-shell nanostructures were dispersed in anhydrous ethanol at a concentration of 1 mg/mL.[3] The target surface density—verified via Atomic Force Microscopy (AFM, JPK Nanowizard)—is achievable through solution concentration and deposition cycles; specifically, lower concentrations require a higher N, whereas higher concentrations reduce the total deposition time. This control over surface density enables dense enough nanoparticle coverage for high color purity while avoiding excessive optical interference between neighboring particles. Material morphology and nanoparticle

distribution were characterized using transmission electron microscopy (TEM, JEOL-2100). Optical transmission and reflection spectra were recorded from 300 to 1000 nm using a home-built system with an integrating sphere (Labsphere). Current-voltage (I-V) characteristics of the integrated SiPG@Solar cell modules were measured under AM 1.5G illumination 100 mW/cm^2 using a large-area Class AAA solar simulator (G2V Optics “Sunbrick”). External quantum efficiency (EQE) spectra were acquired using the same LED-based solar simulator when specific color diodes were selectively used. Color coordinates were derived from the reflectance spectra and mapped into the CIE 1976 (u'v') uniform chromaticity scale. To characterize device performance, we integrated the SiPG structures with high-efficiency monocrystalline silicon modules (SM451K08L, ANYSOLAR Ltd.)

Figure S1

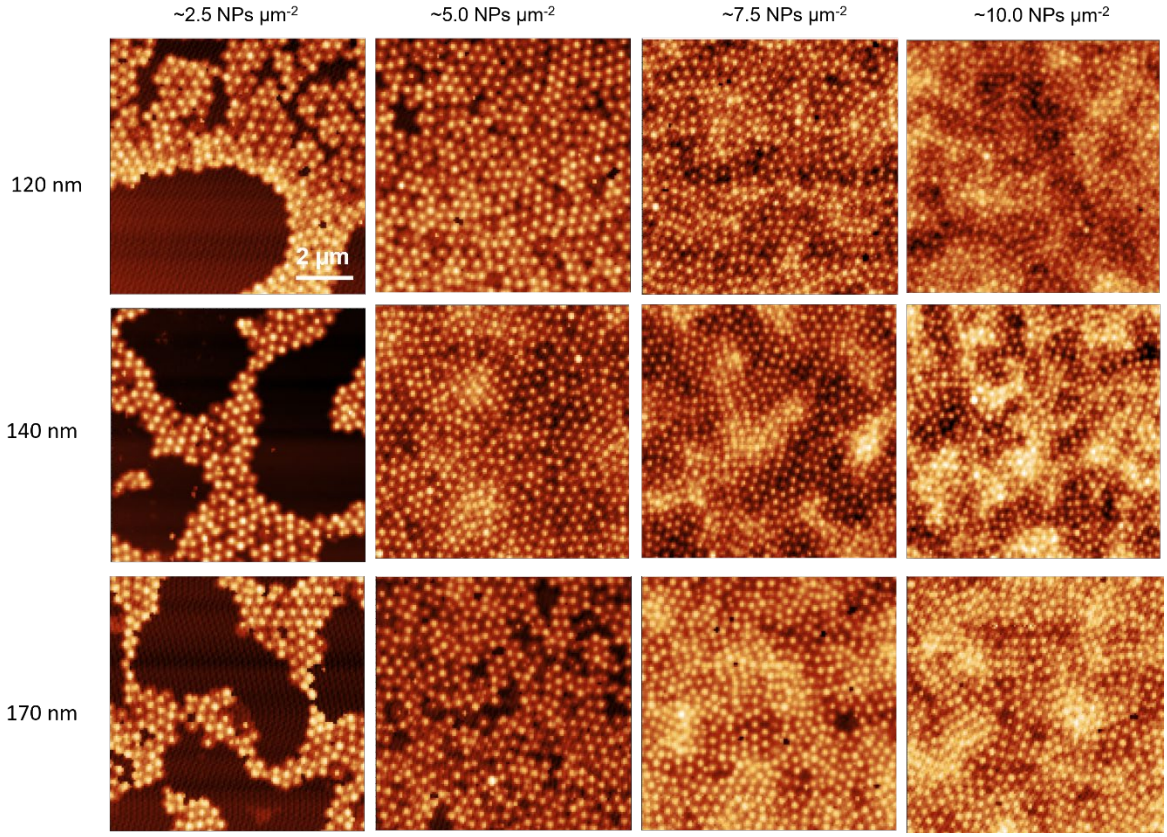

Figure S1: Morphological characterization and density control of Si NP layers. AFM images of Si NPs (120, 140, 170 nm) across four target surface densities (2.5-10.0 NPs μm^{-2}) fabricated via slot-die coating. The labels represent averaged densities, accounting for local variations of ±1.0-1.5 NPs μm^{-2} inherent to large-area processing. Precision control of the sub-monolayer distribution is achieved by modulating solution concentration and the number of coating passes.

Figure S2

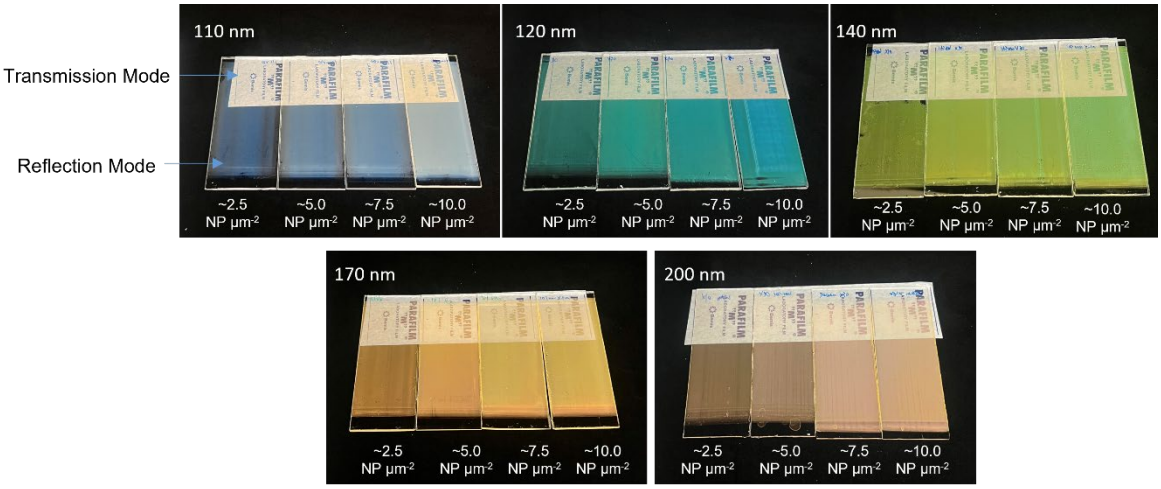

Figure S2: Visual validation of transmission and reflection modes in SiPGs. Photographs of SiPGs across various Si NP diameters (110–200 nm) and surface densities (2.5-10.0 NPs μm^{-2}). Images captured against a non-reflective black background with standardized white balance calibration demonstrate the contrast between selective reflection and high-transmission modes.

Figure S3

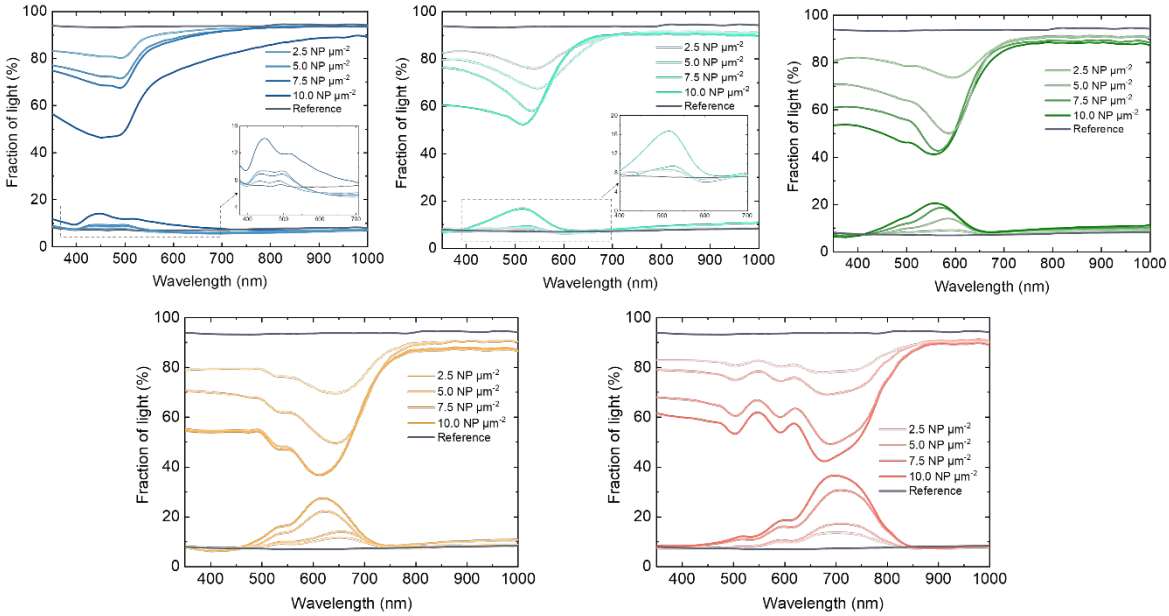

Figure S3: Density-dependent spectral tunability of SiPGs. Transmittance and reflectance spectra for SiPGs with Si NP diameters of 110, 120, 140, 170, and 200 nm across surface densities from ~2.5 to 10.0 NPs μm^{-2}. Insets highlight the reflectance of intensity modulation in the visible regime.

Figure S4

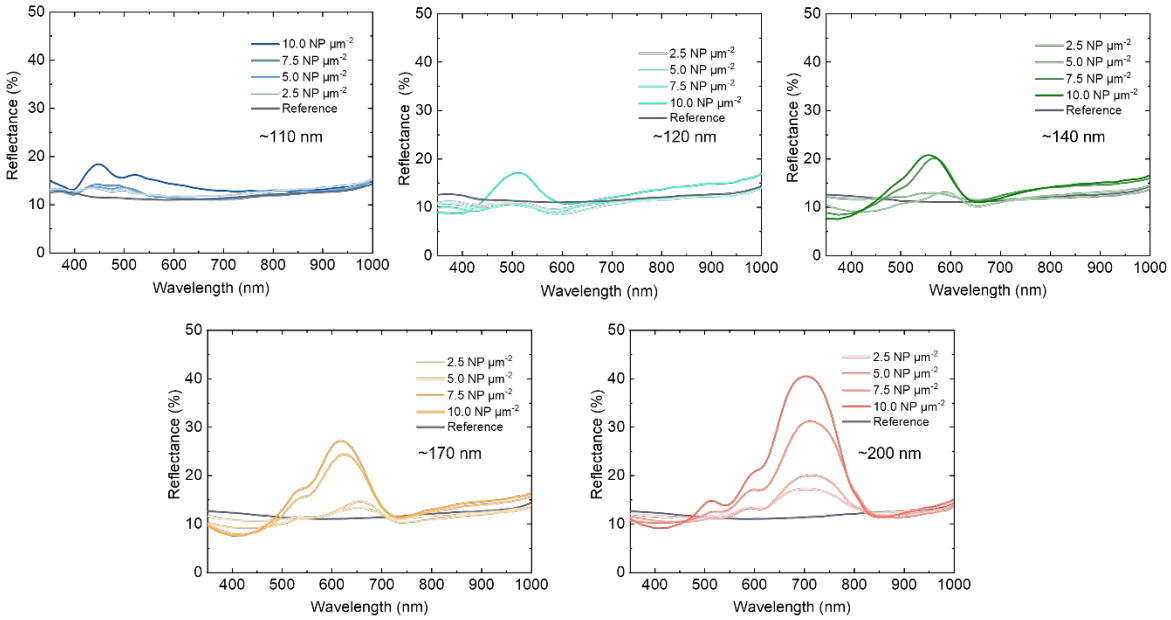

Figure S4: Integration-induced reflectance evolution of SiPG@PV modules. Reflectance spectra of integrated SiPG@PV modules for Si NP diameters of 110, 120, 140, 170, and 200 nm across surface densities from ~2.5 to 10.0 NPs μm^{-2}.

Figure S5

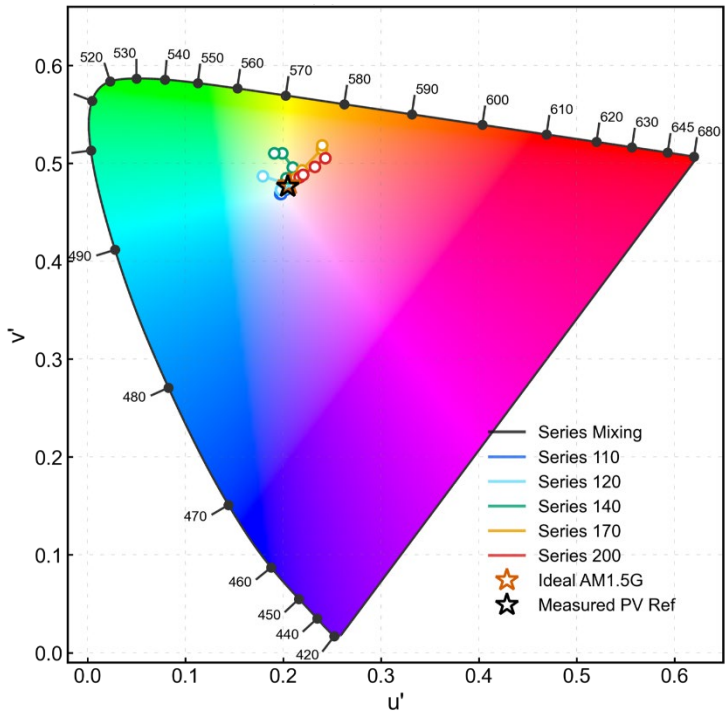

Figure S5: Chromaticity coordinates and color gamut of SiPG@PV modules. CIE 1976 (u', v') chromaticity diagram showing the color gamut achieved by integrated SiPG@PV modules. The orange and black stars represent the ideal AM1.5G and measured PV references, respectively. Data points track the spectral evolution of the 110, 120, 140, 170, 200 nm and 120+200 nm mixing series, illustrating the shift from the neutral white point toward saturated color regions as surface density increases from ~2.5 to 10.0 NPs μm^{-2}.

Figure S6

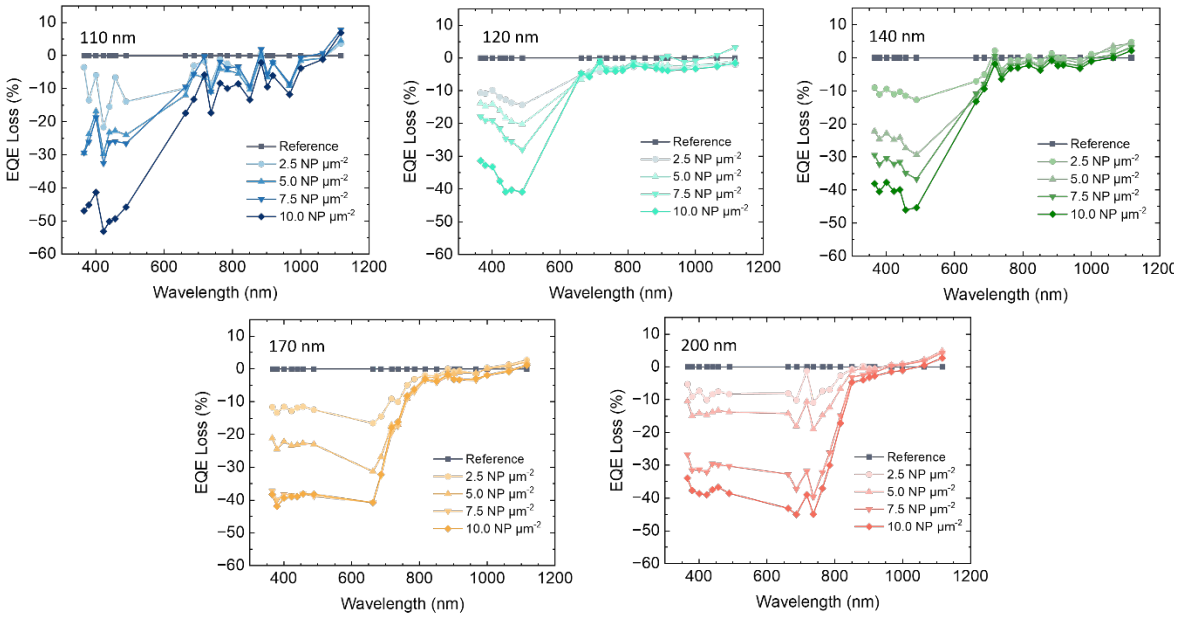

Figure S6: Spectral EQE loss analysis as a function of Si NP surface density. Wavelength-dependent External Quantum Efficiency (EQE) loss for SiPG@PV modules with Si NP diameters from 110 nm to 200 nm. For each particle size, the EQE loss is plotted across four surface densities (~2.5-10.0 NPs μm^{-2}), relative to a standard PV reference.

Figure S7

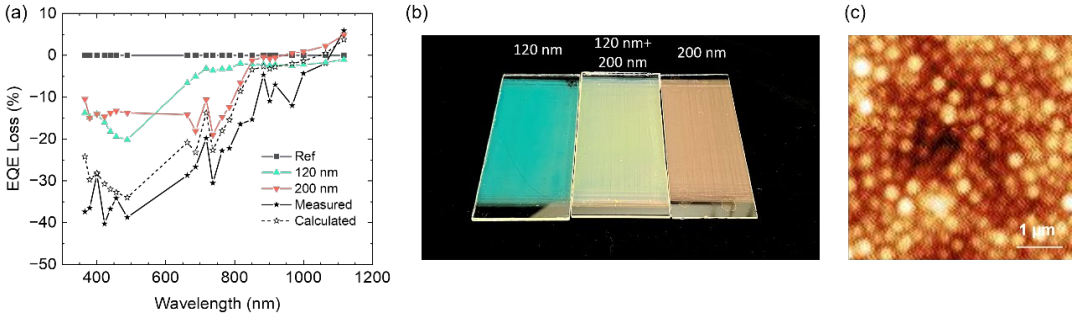

Figure S7: Color mixing through binary Si NP blending. (a) EQE loss spectra comparing the 120 nm and 200 nm (~5.0 NPs μm^{-2} for each sample) primary series with their mixed blend at a total surface density of 10.0 NPs μm^{-2}. (b) Photograph of the 120 nm, 200 nm, and 120+200 nm mixed samples, demonstrating the generated intermediate hue. (c) AFM image of the mixed Si NP sub-monolayer.

Figure S8

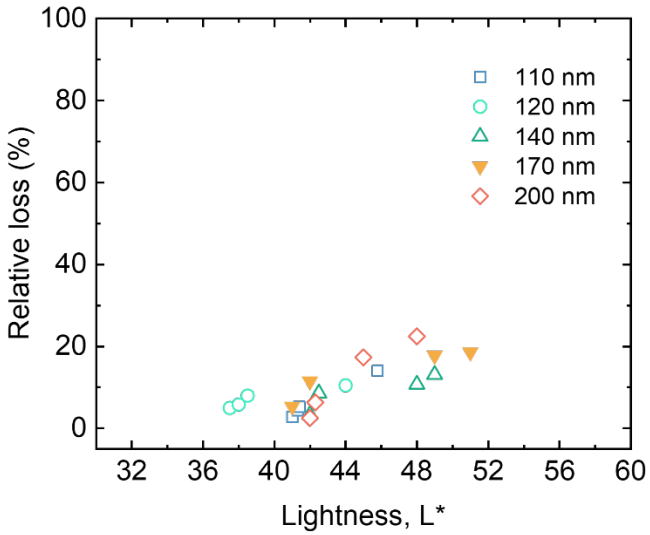

Figure S8: Correlation between photocurrent loss and visual lightness. Relative photocurrent loss as a function of the CIELAB L^* (lightness) value for various Si NP diameters. The data points represent the trade-off between electrical performance and the perceived brightness of the colorful PV modules.

References

[1] O. Vu, J. Song, H. Sugimoto, and M. Fujii, “Polymer-Shell Coating of Mie-Resonant Silicon Nanospheres for Controlled Fabrication of Self-Assembled Monolayer,” ACS Appl. Nano Mater. **8**(29), 14802–14810 (2025).

[2] H. Tanaka, S. Hotta, T. Hinamoto, H. Sugimoto, and M. Fujii, “Monolayer of Mie-Resonant Silicon Nanospheres for Structural Coloration,” ACS Appl. Nano Mater. **7**(3), 2605–2613 (2024).

[3] Z. Song, X. Lu, O. Vu, J. Song, H. Sugimoto, M. Fujii, L. Berglund, and I. Sychugov, “Selective scatterers improve efficiency and color neutrality of semitransparent photovoltaics,” ACS Photonics **12**(11), 6458–6467 (2025).